Batteries & Supercaps

Research Article
doi.org/10.1002/batt.202300433

Chemistry Europe
European Chemical Societies Publishing

www.batteries-supercaps.org

Lithium-Sulfur Batteries with Triethylsulfonium Bis(trifluoromethane sulfonyl)imide Ionic Liquid During First Charge-Discharge Cycling: EIS & DFT Study

M. Pushpa Selvi,[a] R. Nimma Elizabeth,*[a] S. Sinthika,[a] S. Arockia Shyamala Paniyarasi,[a] S. Padmaja,[a] and S. Susanna Victoria Backiyaleela[a]

With high theoretical capacity and energy density, lithium-sulfur batteries (Li–S) have the potential to meet future energy demands including electric vehicles. Various strategies have been developed to address the challenges of Li–S batteries such as polysulfide shuttling, capacity fading, and lithium dendrite formation. By using suitable electrolyte additives, it is possible to enhance the interfacial properties of Li–S batteries and mitigate polysulfide shuttling. In the present work, an aprotic ionic liquid Triethylsulfonium bis(trifluoromethane sulfonyl)imide ($[S_{222}][TFSI]$) has been used as an electrolyte additive, and the physico-electrochemical and interfacial properties are investigated. The Li||Li cell with hybrid electrolyte shows stable interfacial resistance and the EIS study during the first discharge and charge of Li–S cell demonstrates stable charge transfer and bulk resistances which indicate the enhanced interfacial properties and the inhibition of polysulfide shuttling. The first-principles calculations were conducted to investigate the nature of the interaction between the lithium polysulfides (LiPSs) and the $[S_{222}][TFSI]$ molecule. Long chain LiPSs (Li_2S_x, $4 < x < 8$) interact with $[S_{222}][TFSI]$ molecule via Li-bond and hyperconjugation effect. $[S_{222}][TFSI]$ shows the ability to dissolve Li_2S and Li_2S_2 precipitation at the cathode surface which can result in increased utilization of active sulfur and reduced capacity fading.

Introduction

The increase in energy demand and the alarming rate of depletion of fossil fuel at the global level have imposed great pressure in the field of batteries towards the design of better energy storage and conversion devices. Though lithium-ion batteries rule the world of batteries, their low specific capacity and safety issues limit their applications in electric vehicles, etc. Lithium-sulfur (Li–S) batteries gain attention because of their high energy density of up to 2600 Wh kg^{-1}, their low cost, and their environment friendliness.[1–4] However, the main challenges obscuring the practical use of Li–S batteries are self-discharge, the low conductivity of sulfur, dissolution of lithium polysulfides (LiPSs) in the electrolyte causing polysulfide shuttle between the electrodes and mysterious electrode/electrolyte interfacial properties.[4]

One of the most common approaches to solve the aforementioned issues is using carbon-based cathode hosts to enhance the conductivity of sulfur and trap lithium polysulfides. Carbon-based structures including graphene,[5–9] graphene oxide,[10] carbon nanotubes,[11,12] carbon fibers,[7] and micro-porous carbon[8] have shown immense potential as cathode hosts for trapping LiPSs. A recent study employed machine learning techniques to identify combinations of single-atom catalyst (SAC) and nitrogen-doped graphene that demonstrated a balance in the inhibition of the shuttle effect while maintaining a low overpotential.[15]

Li–S cells with commercial liquid electrolytes suffer from self-discharge and polysulfide shuttle.[16] Although replacing the nonaqueous liquid electrolytes with solid[17] and gel polymer electrolytes[18] shows improved performance, the solid electrolytes suffer from poor electrode/electrolyte interfacial properties and poor Li^+ diffusion.[11,12] Appropriate electrolyte additives can contribute to the formation of a stable solid electrolyte interface (SEI) and reduce the deposition of insoluble lithium polysulfides such as Li_2S and Li_2S_2. Attempts have been made to overcome the polysulfide shuttling and retain the capacity using suitable solvents, supporting lithium salt, and electrolyte additives.

$LiNO_3$ additive in electrolytes has been identified to enhance the interfacial properties by forming a stable solid electrolyte interphase (SEI) on the lithium anode.[21,22] Yet, the deposition of insoluble short-chain lithium polysulfides on the Li anode[23] and the dissolution of lithium long-chain polysulfides in the electrolyte lead to loss of active sulfur and capacity fading. In recent studies, hybrid electrolytes have shown stable interfacial resistance, high rate capability, and faster Li^+ transport.[24,25]

Therefore, a suitable electrolyte additive that enhances the interfacial properties and also offers reduced solubility to long-chain lithium polysulfides is essential for high-performance lithium-sulfur batteries. Room temperature ionic liquids (RTILs) are known for their excellent ionic conductivity comparable to

[a] M. Pushpa Selvi, Dr. R. Nimma Elizabeth, Dr. S. Sinthika, Dr. S. Arockia Shyamala Paniyarasi, Dr. S. Padmaja, S. Susanna Victoria Backiyaleela
Department of Physics and Research Centre
Lady Doak College (Autonomous),
Affiliated to Madurai Kamaraj University, Madurai
Tamil Nadu 625002 (India)
E-mail: nimmaelizabeth@ldc.edu.in

Supporting information for this article is available on the WWW under https://doi.org/10.1002/batt.202300433

Research Article
doi.org/10.1002/batt.202300433
Chemistry Europe
European Chemical Societies Publishing

many organic electrolytes used in lithium batteries, better thermal stability, and negligible vapor pressure.[26–28] Studies have shown that ILs also contribute to the formation of stable SEI at the electrode.

Symmetric and asymmetric trialkylsulfonium cations are useful for producing RTILs with relatively low shear viscosities and competitive ionic conductivities.[29] The cationic structure in the triethylsulfonium RTILs leads to favourable physical-chemical properties for lithium ion based applications.[30] In the present work, an aprotic room temperature ionic liquid triethylsulfonium bis (trifluoromethane sulfonyl)imide ([S_{222}][TFSI]) has been used as an electrolyte additive and its electrochemical and interfacial properties in enhancing the electrochemical performance of the Li–S batteries is explored.

Results and Discussion

Morphological analysis of S/MWCNT composite

The prepared S/MWCNT composite material was characterized by XRD and Raman spectroscopic methods to confirm the composite structural formation. The XRD patterns of sulfur exhibit the characteristic features of the Fddd orthorhombic structure. The characteristic peaks of the S/MWCNT composite are observed at 15°, 23°, 26° and 31° corresponding to (1 1 3), (2 2 2), (0 2 6), and (0 4 4) planes respectively and they are consistent with that of the elemental sulfur, which indicates no phase transformation of sulfur has been observed in the composite structure (Figure 1Ac). The absence of a MWCNT peak corresponding to the (0 0 2) plane confirms that the sulfur has covered the CNT surface. In the Raman spectrum shown in Figure 1(B), the D-band (1353 cm^{-1}), G-band (1584 cm^{-1}), and D′-band, the second order overtone of D-band (2699 cm^{-1}) confirms the typical characteristics of MWCNT.[31] The low-intensity ratio of D and G bands (I_D/I_G) shows good purity MWCNT present in the sample.

The surface morphology of the prepared cathode was obtained using SEM and the composition was confirmed using EDAX (Figure 2a and b). Figure 2(c–h) shows the TEM and SAED analysis of S/MWCNT nanocomposite. Figure 2(c) shows the sulfur nanoparticles covering the walls of the MWCNT. The formation of a curved graphitic structure (Figure 2f) on the surface of MWCNT shows the structural changes on the outer wall of MWCNT due to the deposition of sulfur nanoparticles. The diameter of MWCNT obtained from TEM is about 12.5 nm and the size of sulfur particles is approximately 37.5 nm.

Electrochemical analysis

Ionic conductivity

To find the ionic conductivity, Celgard 2320 was soaked in electrolytes and sandwiched between the steel electrodes and EIS was observed for the coin cells with base electrolyte and those with IL. The ionic conductivity of the samples is presented in the Arrhenius plots in Figure 3 at temperatures from 10 °C to 70 °C. It is observed that the hybrid electrolyte containing [S_{222}][TFSI] IL shows higher ionic conductivity (1.1 to 2.45 mS cm^{-1}) than that of the base electrolyte (0.7 to 1 mS cm^{-1}) as the temperature increases from 10 °C to 70 °C.[32]

Open circuit voltage (OCV) and bulk resistance

The evolution of the open circuit voltage is a simple qualitative indicator of the rate of self-discharge in Li–S batteries. Li–S coin cells prepared with selected electrolytes were stored at room temperature and OCV was observed periodically. Figure 4(a) shows that the cell with base electrolyte shows a continuous decrease in OCV from 2.54 to 2.43 V over a period of 18 days. The cell with a hybrid electrolyte containing [S_{222}][TFSI] IL maintains the OCV of 2.58 V from the 7th day onwards which indicates that a stable Cathode Electrolyte Interface (CEI) is formed at the cathode that reduced the self-discharge. The hybrid electrolyte with [S_{222}][TFSI] IL effectively controls the dissolution of polysulfides and the self-discharge compared to the commercial base electrolytes and ionic liquid 1-Allyl-3-methylimidazolium bis(trifluoromethanesulfonyl)imide (AMImTFSI) reported in the recent studies.[16,33,34] This is also evident from the evolution of bulk resistance in the cells as

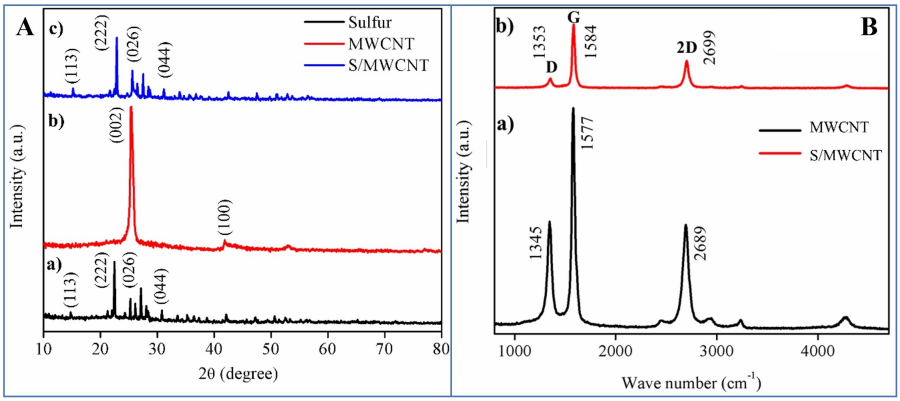

Figure 1. A. X-ray diffraction patterns of (a) Sulfur (b) MWCNT (c) S/MWCNT B. Raman spectra of (a) MWCNT (b) S/MWCNT.

Research Article
doi.org/10.1002/batt.202300433
Chemistry Europe
European Chemical Societies Publishing

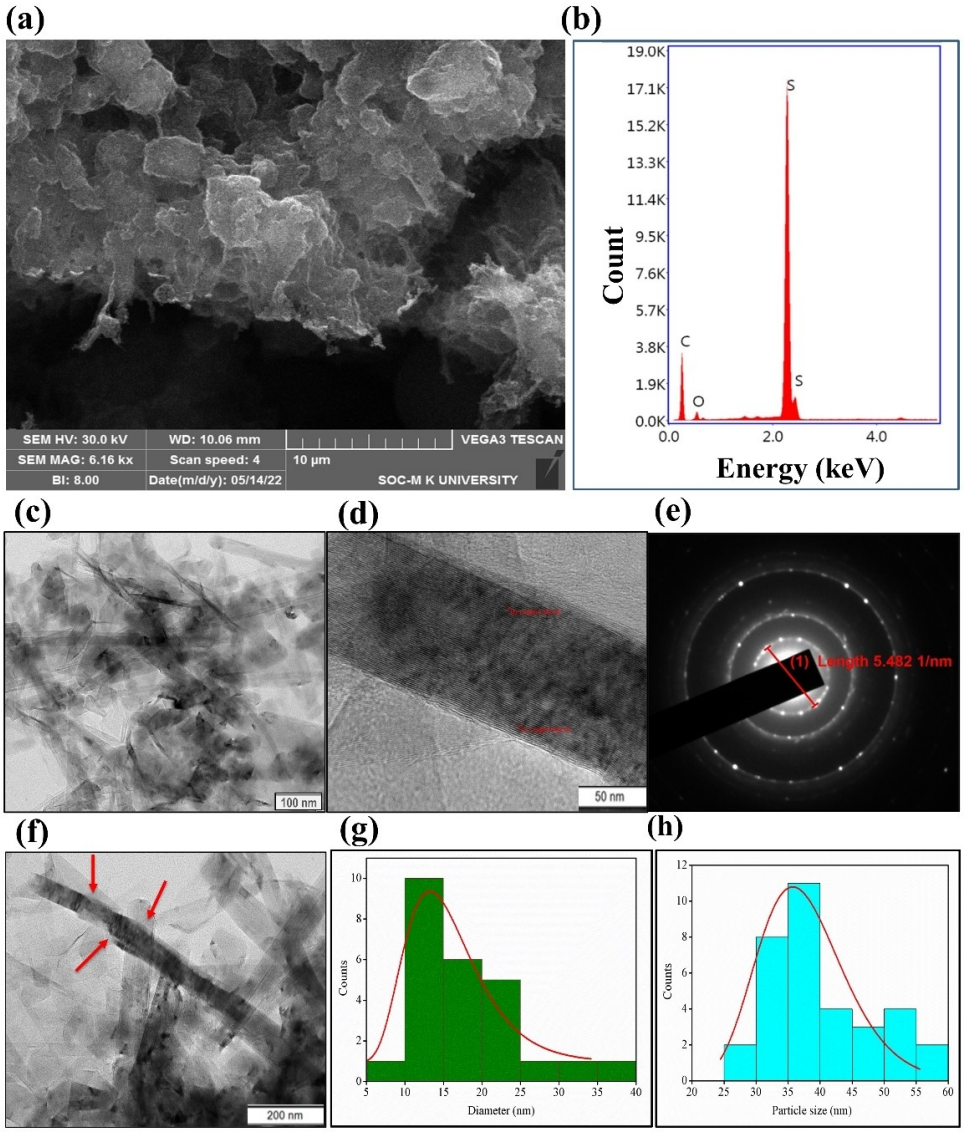

Figure 2. a and b) SEM Analysis of S/MWCNT cathode. c–h) TEM analysis of S/MWCNT composite. c,d and f) TEM images, e) SAED pattern and g,h) particle size histograms of MWCNT and S, respectively.

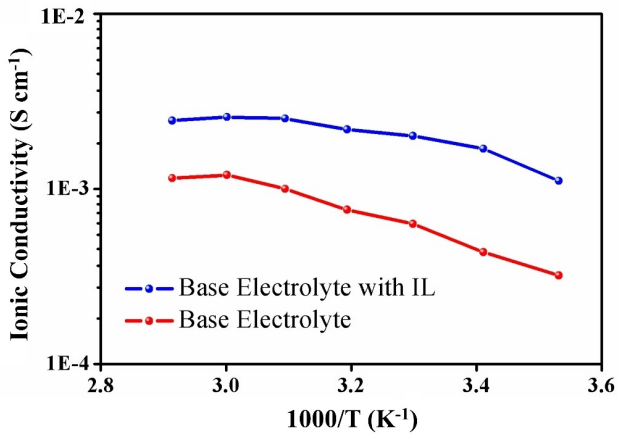

Figure 3. Arrhenius plot showing the ionic conductivity vs. temperature of electrolytes with and without ionic liquid [S_{222}][TFSI].

shown in Figure 4(b). Bulk resistance is the electrolyte resistance that relies on the concentration and composition of electrolyte which includes the solvents, additives, and dissolved polysulfide species. Low and constant bulk resistance represents an electrolyte with no contamination of polysulfides. [S_{222}][TFSI] added electrolyte shows small bulk resistance compared to the base electrolyte (Figure 4b). Constant bulk resistance (≈4.2 Ω) after the 12th day of storage also indicates that the lithium polysulfide dissolution is controlled by CEI effectively in the cell with [S_{222}][TFSI].

Cyclic voltammetry (CV) study

A cyclic voltammetry study was carried out to understand the effect of ionic liquid in redox reactions. The first two cycles of cyclic voltammogram observed between potentials of 1.5–3 V

Research Article
doi.org/10.1002/batt.202300433
Chemistry Europe
European Chemical Societies Publishing

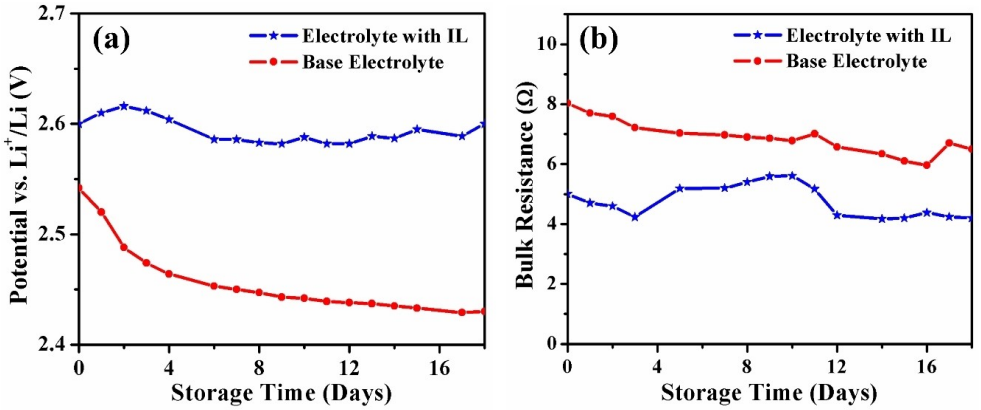

Figure 4. Evolution of a) Open circuit voltage and b) bulk resistance in Li–S cell.

with the scan rate of 0.1 mV/s for the cells with selected electrolytes are displayed in Figure 5(a and b).

CV with IL containing electrolyte (Figure 5a) shows two reduction peaks in the cathode scan at 2.37 V and 1.97 V, owing to the conversion of cyclic S_8 to long-chain LiPSs (Li_2S_x, $4 < x < 8$) and reduction of long-chain polysulfides to short-chain LiPSs (Li_2S_x, $1 < x < 4$) respectively.[35] The single anodic peak present at 2.45 V for the electrolyte with IL is ascribed to the combined conversion of lithium sulfide to lithium polysulfides and finally to the formation of Li_2S_8.

Overlapping of redox peaks for 1st and 2nd cycles for the hybrid electrolyte (Figure 5a) confirms the reduced polarization effect in the cell resulting in high reversibility.[36] It is also evident from the smaller value of anodic and cathodic peak difference ΔE_p (0.08 V for electrolyte with IL and 0.24 V for base electrolyte). The peaks of Li–S cell with hybrid electrolyte containing IL are sharp which indicates fast kinetics in the cell.[37]

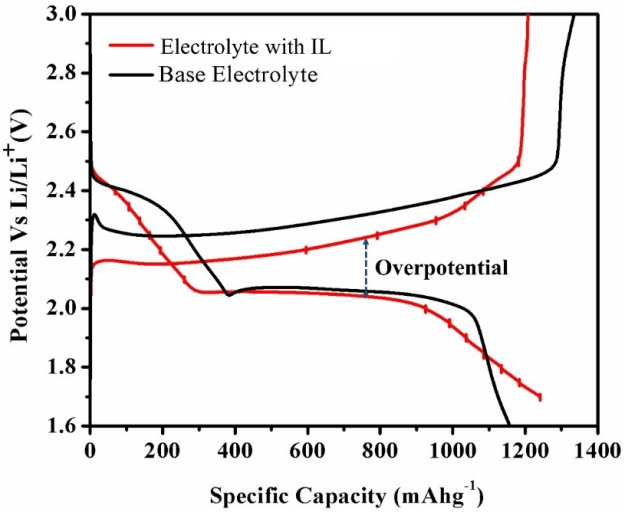

Figure 6. First cyclic charge-discharge profile of Li–S cells with base electrolyte and IL containing electrolyte.

Galvanostatic cycling

The first cycle of charge-discharge profiles of Li–S cells at 0.1 C are shown in Figure 6. An almost symmetric profile with a specific capacity of 1200 mAh g^{-1} was observed for the cell with $[S_{222}][TFSI]$ IL containing electrolyte. Small ΔE between the charge and discharge curves represents fast reaction kinetics in the cell compared to the cells with base electrolyte, piperidi-

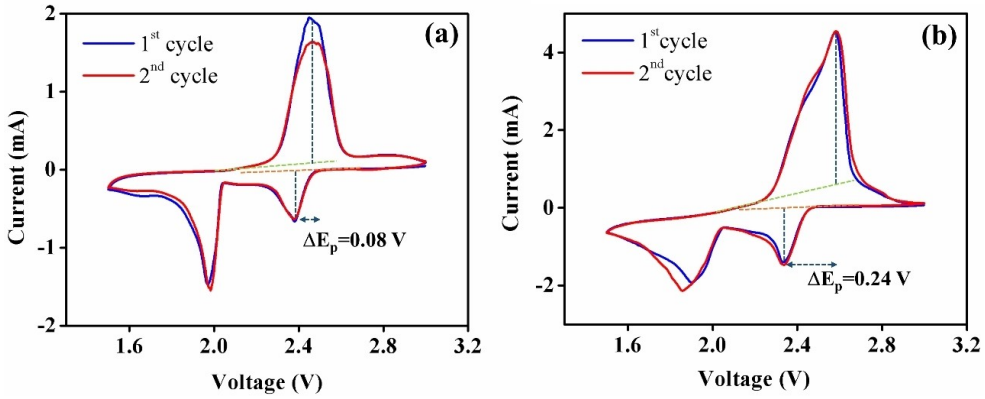

Figure 5. Cyclic voltammograms of Li–S cells with a) $[S_{222}][TFSI]$ containing electrolyte, and b) base electrolyte.

Research Article
doi.org/10.1002/batt.202300433
Chemistry Europe
European Chemical Societies Publishing

nium and imidazolium-based ionic liquids.[33,34,38,39] Also, the cell with IL shows a relatively short high voltage plateau, which might have been caused by the presence of the strong polysulfide shuttle, which prevents the cell from being fully charged and causing low self-discharge in this region.[40] It is also observed that the cell with IL exhibits a smaller charge overpotential compared to the discharge overpotential. This can be attributed to the interaction between the $[S_{222}][TFSI]$ molecule and Li_2S. The strong binding between the [TFSI] anion and Li_2S causes an elongation of the Li–S bond. This elongation decreases the activation energy of Li_2S, consequently lowering the charge overpotential.[41] The DFT calculations also confirm the strong interaction of Li_2S with ionic liquid (Figure 11a).

Electrode/electrolyte interfacial properties

Compatibility

The electrolyte and additives play an important role in the formation of solid electrolyte interface (SEI) which is critical in the electrochemical performance of a Li–S battery. A stable interface forbids the formation of lithium dendrites at the anode surface and ensures better performance of a battery. To obtain a better understanding of the interfacial properties of lithium anode/electrolyte, the Li||Li symmetric cells were assembled with base and $[S_{222}][TFSI]$ IL-added electrolytes. The cells were stored at room temperature and EIS spectra were observed periodically. The real axis intercept at a high frequency is ascribed to the electrolyte resistance (R_{bulk}) and the semicircle appearing from high to medium frequencies represents the interfacial resistance (R_{SEI}). Figure 7(a) shows that the interfacial resistance due to the base electrolyte continuously varies and it agrees with the experimental observations conducted earlier.[16] This indicates the formation of unstable SEI whereas the electrolyte with $[S_{222}][TFSI]$ IL shows a lower and almost constant interfacial resistance after the third day. The stable and low interfacial resistance is significant compared to the results obtained with 1-ethyl-3-methylimidazolium bis(trifluoromethylsulfonyl) imide (EMITFSI) IL.[42]

Dendrite study

The growth of lithium dendrites on the anode surface during the subsequent charge-discharge cycling mainly depends on the quality and stability of the SEI layer formed on the anode when the electrode and electrolyte are brought into contact in a freshly fabricated coin cell. A stable and homogenous SEI can inhibit the growth of lithium dendrites and ensure the safety of Li–S batteries from short circuits.[36] To evaluate the effect of IL, on the stability of the electrode-electrolyte interface towards the suppression of lithium dendrites, a lithium plating/stripping study was carried out. Li||Li symmetric cells with the selected electrolytes were cycled under the constant current density of 0.1 mA cm^{-2} under 60 min charging/discharging at room temperature and the overpotentials were calculated. Figure 7(b) shows that the cell with base electrolyte shows an overpotential of ≈0.013 V and an addition of $[S_{222}][TFSI]$ IL reduced the overpotential to ≈0.006 V. Further, a constant overpotential even after 200 hours indicates the steady rate of stripping and plating which is attributed to the stable SEI formed at the interface.[44]

EIS study of Li-S cell during first charge-discharge

Electrochemical Impedance spectroscopy is a simple and powerful tool to study the electrochemical performance of batteries during charge-discharge. An in-depth understanding of electrolyte resistance, formation of the electrode-electrolyte interface, polysulfide diffusion, etc. can be obtained using EIS.[45]

Impedance spectra of the cell represent the several physical and electrochemical processes occurring simultaneously in the battery which can be seen from the semicircles and Warburg elements. The number of semicircles in the EIS of Li–S depends on the depth of discharge/state of charge.[45] Li–S cells were assembled with the selected electrolyte and cycled at a constant current rate of 0.1 C and EIS spectra were recorded at different cell potentials during the first discharge and charge process. Figure 8(a–d) and (e) shows the Nyquist plot of EIS spectra recorded for the cell with hybrid electrolyte and base

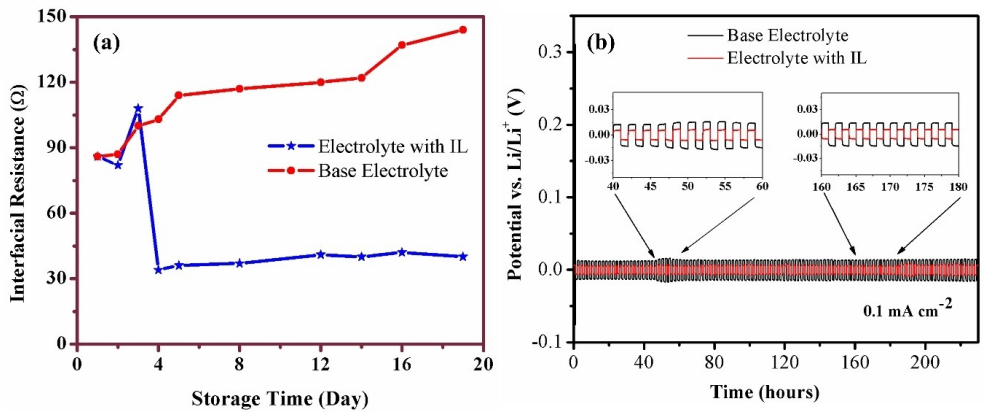

Figure 7. a) Interfacial resistance of Li||Li symmetric cells. b) Voltage-time profile of lithium plating/stripping in a Li/Li symmetrical cell at a constant current density of 0.1 mA cm^{-2} with base and hybrid electrolytes.

Research Article
doi.org/10.1002/batt.202300433
Chemistry Europe
European Chemical Societies Publishing

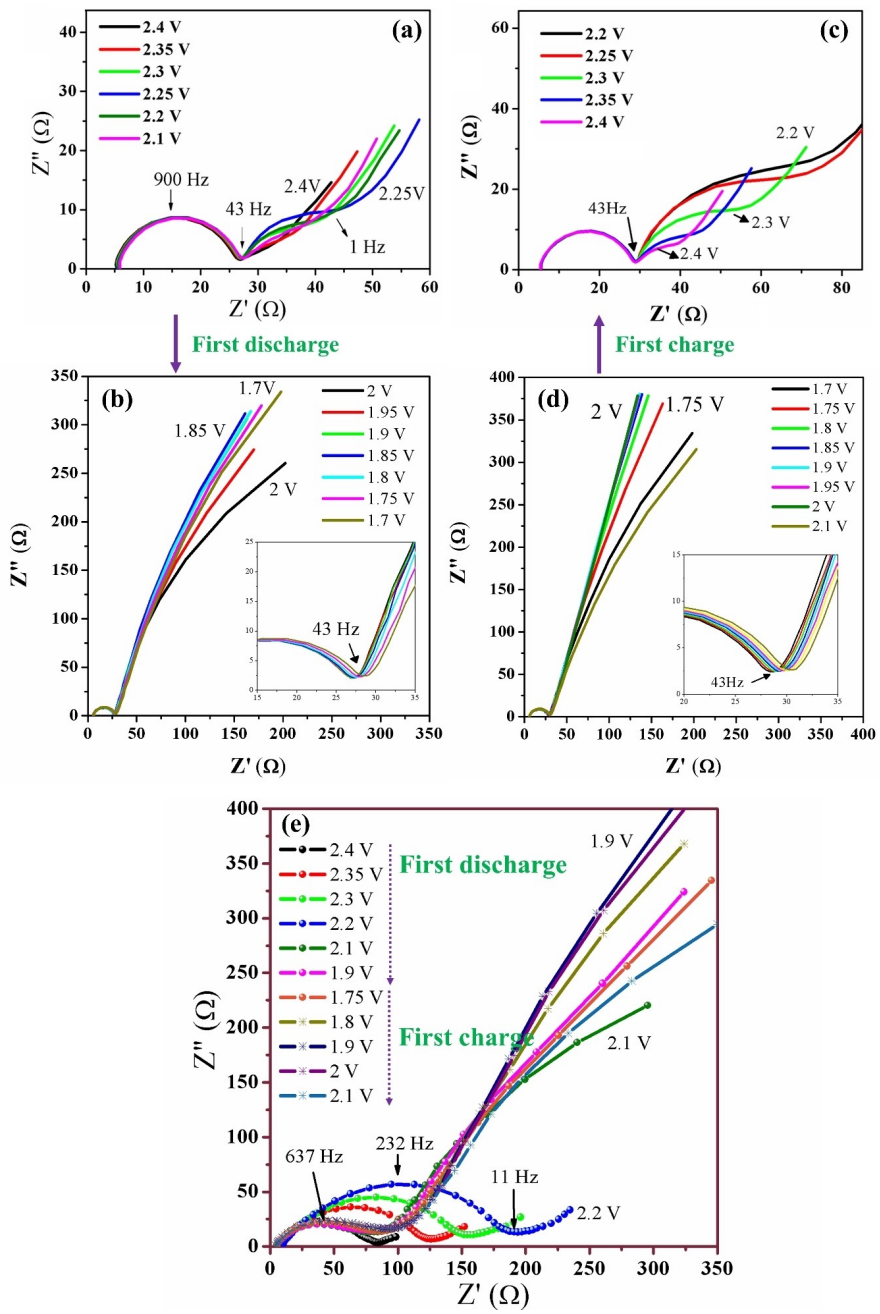

Figure 8. Evolution of Nyquist plot observed at different cell potentials during first discharge and charge of the Li/S cells a–d) with ionic liquid containing electrolyte, and e) with base electrolyte.

electrolyte, respectively. The Li–S cell exhibited two distinctive trends of EIS spectrum corresponding to high and low voltage plateau (2.4–2.1 V & 2–1.7 V) during the first discharge and charge. The real axis intercept at the high frequency region is the bulk resistance (R_{bulk}) contributed mainly by the electrolyte, the semicircle at the mid frequency region is attributed to the passivation layer formed at the lithium anode surface.[16] Figures 8(a–d) & 9(a and b) reveal that the charge transfer resistance remains constant throughout the first discharge and charging process in the cell incorporating [S_{222}][TFSI]. In contrast, the cell with the base electrolyte experiences a significant increase in R_{ct} during discharge as in Figure 8(e). This rise in R_{ct} is likely attributed to the deposition of insoluble polysulfides on the Lithium surface. It indicates the higher rate of dissolution of polysulfides in the base electrolyte compared to the electrolyte containing [S_{222}][TFSI] IL.[46]

FTIR Analysis

FTIR analysis of lithium anode was performed to investigate the influence of the ionic liquid on the formation of the solid

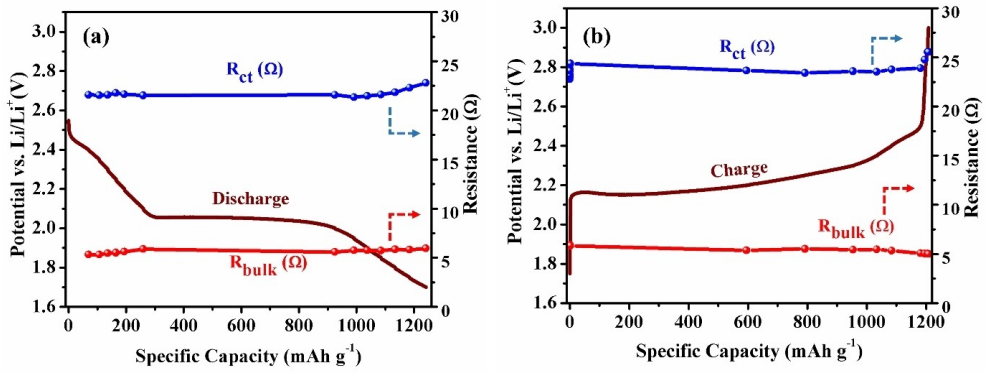

Figure 9. Evolution of a) charge transfer resistance (R_{ct}) and b) bulk resistance (R_{bulk}) observed at different cell potentials during the first discharge and charge of the Li–S cells with IL containing electrolyte.

electrolyte interface (SEI). Following the first galvanostatic cycling, Li–S coin cells were disassembled, and the FTIR spectrum of the lithium anode was examined (Figure S1). Peaks at 1750 cm^{-1}, 1675 cm^{-1}, 1215 cm^{-1}, 860 cm^{-1}, and 3700 cm^{-1}, corresponding to C=O, C=C, C–O, Li–O, and O–H vibrations, were observed in both cells with the base electrolyte and hybrid electrolyte.[47–49] These peaks originate from the interaction of solvents (DOL and TEGDME) and the lithium salt (LiTFSI) with the lithium anode.

Notably, the intensity of the peak associated with the C–SO_2–N vibration of the TFSI ion at 1335 cm^{-1} is increased, and new peaks corresponding to C–N and S–N have appeared in the SEI. This observation supports the involvement of [S_{222}][TFSI] in SEI formation.[50] The graph reveals a significant reduction in the intensity of the peak at 953 cm^{-1}, corresponding to Li_2S, in the electrolyte containing [S_{222}][TFSI]. This disappearance suggests the formation of a stable SEI and effective control of the polysulfide shuttle in the presence of [S_{222}][TFSI].[34]

Computational approach

To explore the nature of the interaction of ionic liquid [S_{222}][TFSI] with lithium polysulfides and its impact on the electrochemical performance of a Li–S battery, DFT calculations were carried out to probe the interaction of [S_{222}][TFSI] molecule with LiPSs. Quantum chemical calculations were performed using the density functional theory (DFT) method with Becke's three parameters (B3) exchange functional and Lee-Yang-Parr (LYP) nonlocal correlation functional (B3LYP). All the structural optimizations were done at the B3LYP/6-31++(d,p) level and the DFT calculations were performed with the Gaussian 09 program package.[51] Molecular electrostatic potential (MEP) was used to identify the reactive sites between the LiPSs and IL molecules.[52] The binding energies of LiPSs with [S_{222}][TFSI] molecule are calculated by using the relation,

$$E_{binding} = E_{tot} - (E_{IL} + E_{LiPS})$$

where E_{tot}, E_{IL}, and E_{LiPS} are the calculated energies of IL molecule bonded with LiPS, ionic liquid, and lithium polysulfide respectively. Charge transfer analysis was done with Natural Bond Orbital (NBO) calculations.

The optimized geometries of LiPSs (Li_2S_x, $1<x<8$) are presented in Figure S2. Molecular Electrostatic Potential (MEP) of the IL molecule and LiPSs are shown in Figure S3, where red and blue regions represent electron-rich and electron-deficient regions, respectively. It can be observed from the figures that the regions where oxygen atoms are situated in IL are electron-rich and the regions of Li^+ in LiPSs are electron-deficient. Hence, the oxygen atoms in the $TFSI^-$ anion of IL are expected to provide nucleophilic attraction for Li^+ attached to LiPSs. The relaxed geometries after the interaction of IL with LiPSs are shown in Figure 10(b–f).

Observations from the optimized geometries in Figure 10(b–f) reveal that one Li atom from all the LiPSs coordinates with two oxygen atoms of $TFSI^-$ anion of the [S_{222}][TFSI] molecule. The binding energy of lithium polysulfides with IL is depicted in Figure 11(a). It is evident that the short-chain polysulfides exhibit strong binding compared to long-chain polysulfides which is a favourable outcome. This preference is important because [S_{222}][TFSI] demonstrates the ability to dissolve Li_2S and Li_2S_2 precipitation of the passive layer which obstructs the active sulfur at the cathode site.[53] This can be explained by examining the highest occupied molecular orbital (HOMO) and lowest unoccupied molecular orbital (LUMO) of LiPSs (Figure S4). In all the lithium polysulfides the HOMO is localized on S atoms. In the case of short-chain LiPSs (Li_2S and Li_2S_2), LUMO is localized on Li atoms, whereas in long-chain polysulfides (Li_2S_4, Li_2S_6, and Li_2S_8) LUMO is localized on S atoms. Therefore, Li atoms of short-chain LiPSs exhibit better charge transferability resulting in stronger binding with IL molecule.[46,53] However, it is worth noting that Figure 11(a) also shows a slight increase in the binding energy of long-chain polysulfides (Li_2S_6 and Li_2S_8).

Li atom of LiPSs interacts with O atoms in the $TFSI^-$ ion of the ionic liquid via a lithium bond which is known to be more of an electrostatic dipole-dipole interaction.[54] The dipole moment of Li_2S and Li_2S_2 are 4.0832 D and 5.1808 D respectively

Research Article
doi.org/10.1002/batt.202300433
Chemistry Europe
European Chemical Societies Publishing

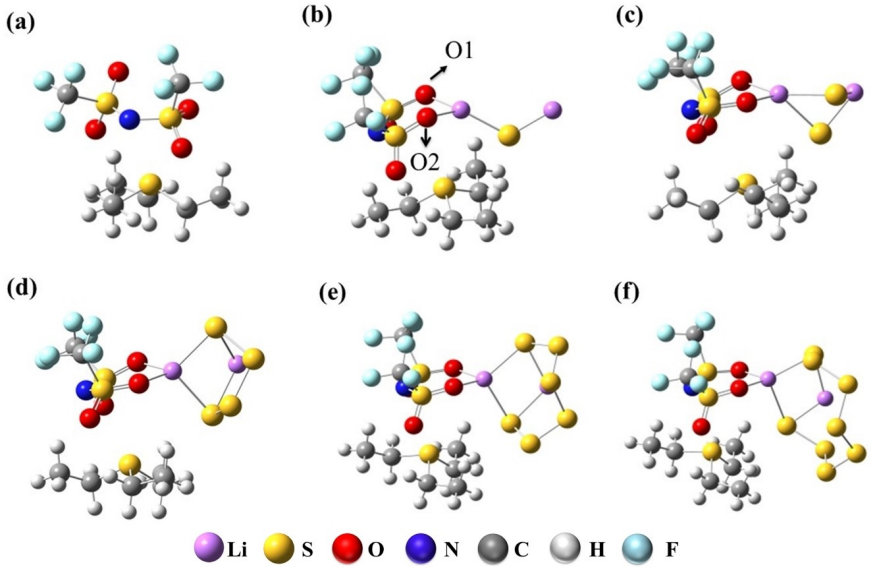

Figure 10. a) Structure of $[S_{222}][TFSI]$ molecule. b–f) Relaxed geometries after the interaction of IL molecule with Li_2S, Li_2S_2, Li_2S_4, Li_2S_6 and Li_2S_8.

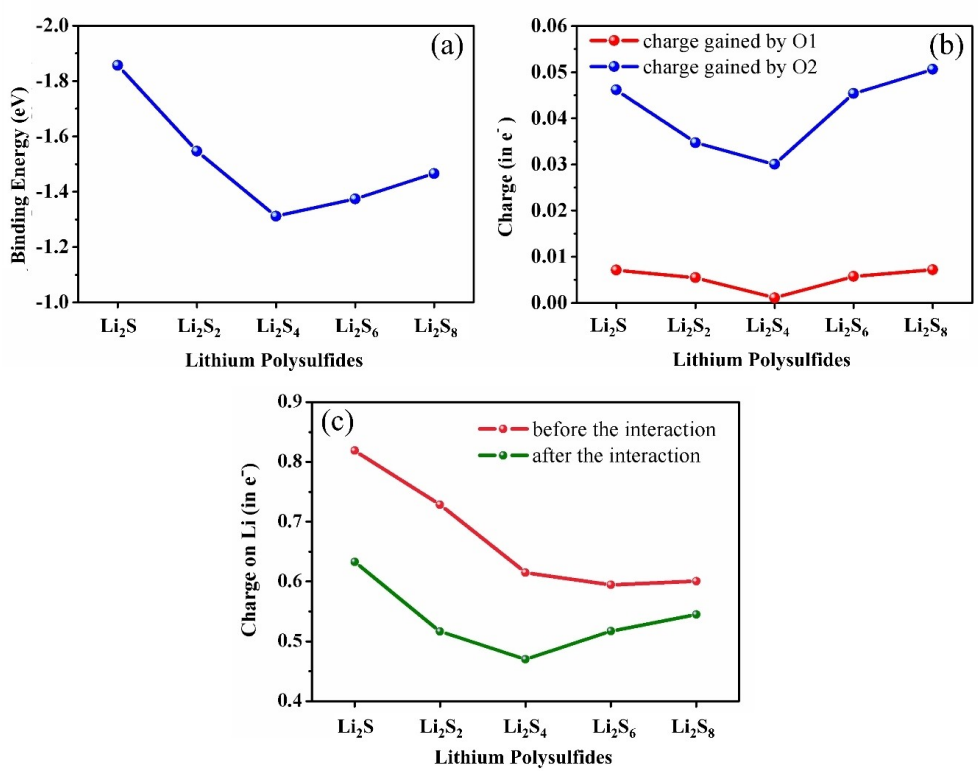

Figure 11. a) The binding energy of lithium polysulfides with $[S_{222}][TFSI]$ molecule. b) Charge gained by the oxygen atoms of $TFSI^-$ anion during the interaction with LiPSs. c) Charge on lithium atom before and after interacting with $[S_{222}][TFSI]$ molecule

which are greater than that of long-chain polysulfides (Li_2S_4 = 2.67 D, Li_2S_6 = 1.12 D and Li_2S_8 = 0.92 D). This is in good agreement with the binding energy for lithium polysulfides. In addition to the dipole-dipole interaction, the charge transfer during the interaction also plays a significant role in the binding strength. Figure 11(b) demonstrates that the charge acquired by oxygen atoms during their interaction with lithium in LiPSs follows a similar pattern as the binding energy.

In order to obtain deeper insight into the nature of interaction between the IL and LiPSs, it is necessary to understand the electronic structure of $TFSI^-$ anion. The structure and the Molecular Electrostatic Potential (MEP) of $[S_{222}][TFSI]$ molecule are shown in Figure S5. The fluorine atoms in the $TFSI^-$

Research Article
doi.org/10.1002/batt.202300433
Chemistry Europe
European Chemical Societies Publishing

anion are highly electronegative which strongly attract electrons. The π electrons of sulfonyl groups are attracted by fluorine atoms. Hence, an oxygen atom from the two sulfonyl groups will be made electron deficient ($^{+}$O-S=O). As a result, one of the S=O bonds from the two sulfonyl groups weakens and one oxygen (O2 in Figure 10b) is electron-rich and the other one (O1 in Figure 10b) is electron deficient. The electron-rich oxygen O2 can bind strongly with Li during the interaction of LiPSs with IL resulting in the lithium bond. The O1 will still bind weakly with Li due to the electron-rich atmosphere (S atoms) of LiPSs.

Natural Population Analysis (NPA) was carried out to investigate the charge transferred during the interaction, during which the sulfur atoms give away the charge that it had already withdrawn from the lithium atom, and the electron-rich oxygen atom of $TFSI^{-}$ anion acquires this charge and binds with the LiPSs. Figure 11(b) illustrates the amount of charge gained by the oxygen atoms of IL which is in good correlation with the binding strength depicted in Figure 11(a). This indicates that the strength of the binding depends on the amount of charge gained by the oxygen atoms which further confirms the electrostatic nature of the lithium bond.[55] Among the two oxygen atoms interacting with the lithium of LiPS, O2 that strongly binds with lithium gains more charge compared to O1 as expected.

It has also been observed that long-chain polysulfides (Li_2S_x, $x=4,6,8$) undergo two distinct interactions with $[S_{222}][TFSI]$ molecule. While the lithium binds with $TFSI^{-}$ anion, the sulfur atoms in LiPSs interact with the methylene group of ethyl substituent present in the TES cation. Since Sulfur in the TES cation is electron deficient and hyperconjugation is expected with the hydrogen of the neighbouring methylenic carbon and makes the methylenic carbon electron deficient. Hence, the hydrogen atom attached to the electron-deficient methylenic carbon undergoes hyperconjugation with the sulfur atom of LiPSs. This interaction weakens the bond between sulfur and lithium, causing lithium to regain some of the charge that it had shared with S earlier. Consequently, oxygen atoms gain more charge, leading to an increase in binding energy for long-chain LiPSs. The charge on the lithium atom before and after interacting with $[S_{222}][TFSI]$ molecule as shown in Figure 11(c) also confirms the above discussion. The schematic representation of the interaction between the long-chain lithium polysulfide and $[S_{222}][TFSI]$ molecule is shown in Scheme 1.

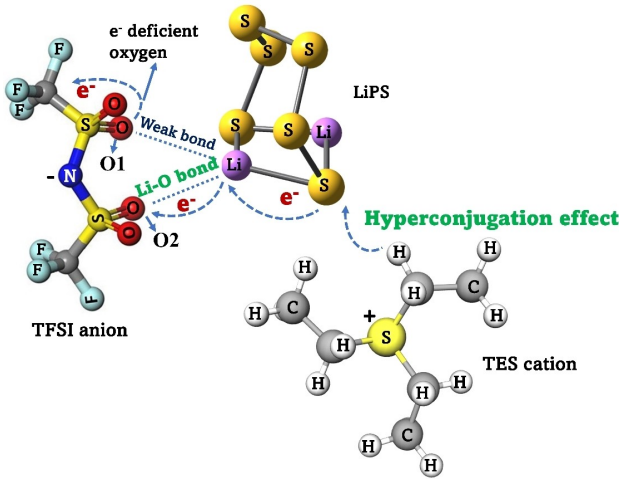

Scheme 1. Interaction of long-chain lithium polysulfides with $[S_{222}][TFSI]$ molecule.

Conclusions

Mitigation of polysulfide shuttling and enhanced interfacial properties are essential for the practical implementation of Li–S batteries. In the present work, a hybrid electrolyte with an ionic liquid additive Triethylsulfonium bis(trifluoromethane sulfonyl)imide was prepared and the physico-electrochemical properties were investigated. The cell with a hybrid electrolyte shows good ionic conductivity, stable interfacial resistance, and low self-discharge. EIS study during the first discharge and charge of the Li–S cell shows stable charge transfer and bulk resistances which indicate the enhanced interfacial properties and the inhibition of polysulfide shuttling. The first-principles calculations were used to investigate the nature of the interaction between the lithium polysulfides (LiPSs) and the $[S_{222}][TFSI]$ molecule. Long chain LiPSs (Li_2S_x, $4<x<8$) interact with $[S_{222}][TFSI]$ via Li-bond and hyperconjugation effect. $[S_{222}][TFSI]$ shows the ability to dissolve Li_2S and Li_2S_2 precipitation at the cathode surface which can result in higher utilization of active sulfur and reduced capacity fading.

Experimental Section

Preparation of S/MWCNT composite and electrode

A S/MWCNT composite was prepared through the melt-infiltration strategy. Sulfur and MWCNT with a mass ratio of 4:1 were mixed uniformly and, the resulting mixture was heated at 156 °C for 9 h to ensure S infiltration on the surface of CNT walls. After being cooled to room temperature, the powder was collected and stored.

The cathodes for Li–S batteries were prepared by mixing 80 wt% of S/MWCNT composite (64 wt% sulfur), 10 wt% carbon black (Super-P), and 10 wt% polyvinylidenedifluoride (PVdF) dissolved in 1-methyl-2-pyrrolidinone (NMP) to form a homogeneous slurry. The slurry was then coated on an aluminium foil using the doctor blade method. The coated electrode was dried at 60 °C and used for the assembly of CR2032 coin cells.

Preparation of electrolyte

Room temperature ionic liquid Triethylsulfonium bis(trifluoromethane- sulfonyl)imide ($[S_{222}][TFSI]$) (TCI, Japan) was used as received. The base electrolyte was prepared by mixing 1,3-dioxolane (DOL) and tetraethylene glycol dimethyl ether (TEGDME) 1:1 (v/v) with 1 M of LiTFSI in an argon atmosphere. The hybrid electrolyte with IL was prepared by mixing $[S_{222}][TFSI]$ with the base electrolyte in a 1:3 (v/v) ratio.

Measurements

Morphological characterization

The prepared S/MWCNT composite material was characterized by XRD (Powder X-Ray Diffractometer – X'Pert Pro – PAnalytic) and Raman (Micro-Laser Raman (Seiki, Japan)) spectroscopic methods to confirm the composite structural formation. The surface morphology of the cathode and its composition were studied with SEM, EDAX, and TEM. The composition of SEI on lithium anode was studied using the FTIR spectroscopic technique.

Electrochemical measurements

Electrochemical impedance spectra (EIS) measurements were performed using a Biologic SP150 electrochemical workstation in the frequency range of 200 kHz to 100 mHz. The galvanostatic cycling of prepared CR2032 coin cells was performed between 1.5 V and 3.0 V at 0.1 C rate at room temperature. Cyclic voltammetry (CV) was also performed on the SP150 electrochemical station between 1.0 and 3.0 V at a scan rate of 0.1 mV s^{-1}.

Supporting Information

Supporting information contains the post-cycling FTIR analysis of the lithium anode, optimized structures of lithium polysulfides, Molecular Electrostatic Potential (MEP) of LiPS and $[_{S222}]$[TFSI] IL and the HOMO and LUMO of lithium polysulfides.

Acknowledgements

The authors acknowledge the University Grants Commission (UGC), New Delhi, India for providing funds under Major Research Grant No. F.No.43-249/2014(SR) to procure the Electrochemical Impedance Analyzer instrument. The authors thank G. Arivazhagan, Department of Physics, Thiagarajar College (Affiliated to Madurai Kamaraj University), Madurai 625009, Tamil Nadu, India for providing access to Gaussian 09 software. The authors acknowledge the contribution of Dr. S. K. Suja, Assistant Professor, Department of Chemistry, Lady Doak College, Madurai, India in analyzing the bonding of LiPS with IL molecule. The authors also thank Dr. Beulah JM Rajkumar, Former head and Associate Professor, Department of Physics, Lady Doak College, and Dr. U. Reeta Felscia, Assistant Professor, Muthurangam Government Arts College, Vellore, Tamil Nadu, for their support to interpret DFT results during the initial stages of the study.

Conflict of Interests

The authors declare no conflict of interest.

Data Availability Statement

The data that support the findings of this study are available from the corresponding author upon reasonable request.

Keywords: lithium-sulfur batteries · DFT · ionic liquid · EIS study · hybrid electrolyte

[1] J.-M. Tarascon, M. Armand, *Issues and challenges facing rechargeable lithium batteries, in: Mater. Sustain. Energy*, Co-Published with Macmillan Publishers Ltd, UK, **2010**, pp. 171–179.
[2] D.-W. Wang, Q. Zeng, G. Zhou, L. Yin, F. Li, H.-M. Cheng, I. R. Gentle, G. Q. M. Lu, *J. Mater. Chem. A 1*. **2013**, 9382.
[3] A. Manthiram, Y. Fu, Y.-S. Su, *Acc. Chem. Res.* **2013**, *46*, 1125–1134.
[4] H. J. Peng, J. Q. Huang, X. B. Cheng, Q. Zhang, *Adv. Energy Mater.* **2017**, *7*.
[5] G. Zhou, E. Paek, G. S. Hwang, A. Manthiram, *Nat. Commun.* **2015**, *6*, 7760.
[6] X. Wang, G. Sun, P. Routh, D.-H. Kim, W. Huang, P. Chen, *Chem. Soc. Rev.* **2014**, *43*, 7067–7098.
[7] Y. Cao, X. Li, I. A. Aksay, J. Lemmon, Z. Nie, Z. Yang, J. Liu, *Phys. Chem. Chem. Phys.* **2011**, *13*, 7660.
[8] H. Wang, Y. Yang, Y. Liang, J. T. Robinson, Y. Li, A. Jackson, Y. Cui, H. Dai, *Nano Lett.* **2011**, *11*, 2644–2647.
[9] S. Feng, Z. Fu, X. Chen, Q. Zhang, *InfoMat.* **2022**, 4.
[10] N. Li, M. Zheng, H. Lu, Z. Hu, C. Shen, X. Chang, G. Ji, J. Cao, Y. Shi, *Chem. Commun.* **2012**, *48*, 4106.
[11] W. Ahn, K.-B. Kim, K.-N. Jung, K.-H. Shin, C.-S. Jin, *J. Power Sources.* **2012**, *202*, 394–399.
[12] X. Ji, L. F. Nazar, *J. Mater. Chem.* **2010**, *20*, 9821.
[13] X. Yang, Y. Yu, N. Yan, H. Zhang, X. Li, H. Zhang, *J. Mater. Chem. A.* **2016**, *4*, 5965–5972.
[14] H.-J. Kang, G. A. K. M. R. Bari, T.-G. Lee, T. T. Khan, J.-W. Park, H. J. Hwang, S. Y. Cho, Y.-S. Jun, *Nanomaterials.* **2020**, *10*, 2012.
[15] Z. Lian, M. Yang, F. Jan, B. Li, *J. Phys. Chem. Lett.* **2021**, *12*, 7053–7059.
[16] S. Waluś, C. Barchasz, R. Bouchet, F. Alloin, *Electrochim. Acta.* **2020**, *359*, 136944.
[17] S. Suriyakumar, S. Gopi, M. Kathiresan, S. Bose, E. B. Gowd, J. R. Nair, N. Angulakshmi, G. Meligrana, F. Bella, C. Gerbaldi, A. M. Stephan, *Electrochim. Acta.* **2018**, *285*, 355–364.
[18] A. Manuel Stephan, *Eur. Polym. J.* **2006**, *42*, 21–42.
[19] T. Welton, *Chem. Rev.* **1999**, *99*, 2071–2084.
[20] M. Armand, F. Endres, D. R. MacFarlane, H. Ohno, B. Scrosati, *Nat. Mater.* **2009**, *8*, 621–629.
[21] D. Aurbach, E. Pollak, R. Elazari, G. Salitra, C. S. Kelley, J. Affinito, *J. Electrochem. Soc.* **2009**, *156*, A694.
[22] X. Liang, Z. Wen, Y. Liu, M. Wu, J. Jin, H. Zhang, X. Wu, *J. Power Sources.* **2011**, *196*, 9839–9843.
[23] B. M. L. Rao, J. A. Shropshire, *J. Electrochem. Soc.* **1981**, *128*, 942–945.
[24] Y.-H. Xu, Q.-F. Zhang, B. Fan, B. Xue, H.-J. Chen, X.-H. Zhang, Z.-K. Luo, F. Wang, D. Le Coq, L. Calvez, H.-L. Ma, P. Fan, *J. Alloys Compd.* **2020**, *845*, 156261.
[25] X. Liu, A. Mariani, H. Adenusi, S. Passerini, *Angew. Chemie Int. Ed.* **2023**, 62.
[26] J.-W. Park, K. Ueno, N. Tachikawa, K. Dokko, M. Watanabe, *J. Phys. Chem. C.* **2013**, *117*, 20531–20541.
[27] A. Lewandowski, A. Świderska-Mocek, *J. Power Sources.* **2009**, *194*, 601–609.
[28] M. Galiński, A. Lewandowski, I. Stępniak, *Electrochim. Acta.* **2006**, *51*, 5567–5580.
[29] S. Fang, L. Yang, C. Wei, C. Peng, K. Tachibana, K. Kamijima, *Electrochem. Commun.* **2007**, *9*, 2696–2702.
[30] H. Haghani, M. Behrouz, V. V. Chaban, *Phys. Chem. Chem. Phys.* **2022**, *24*, 9418–9431.
[31] M. A. S. M. Haniff, S. M. Hafiz, K. A. Wahid, Z. Endut, M. I. Syono, N. M. Huang, S. A. Rahman, I. A. Azid, *J. Mater. Sci.* **2017**, *52*, 6280–6290.
[32] S. Suriyakumar, M. Kathiresan, A. M. Stephan, *ACS Omega.* **2019**, *4*, 3894–3903.
[33] L. Wang, J. Liu, S. Yuan, Y. Wang, Y. Xia, *Energy Environ. Sci.* **2016**, *9*, 224–231.
[34] H. S. Kim, T.-G. Jeong, N.-S. Choi, Y.-T. Kim, *Ionics (Kiel).* **2013**, *19*, 1795–1802.

[35] L. Li, L. Chen, S. Mukherjee, J. Gao, H. Sun, Z. Liu, X. Ma, T. Gupta, C. V. Singh, W. Ren, H. Cheng, N. Koratkar, *Adv. Mater.* **2017**, *29*, 1602734.
[36] Z. Cao, C. Ma, Y. Yin, J. Zhang, Y. Ding, M. Shi, S. Yang, *New J. Chem.* **2015**, *39*, 9659–9664.
[37] D. E. Mathew, S. Gopi, M. Kathiresan, G. J. Rani, S. Thomas, A. M. Stephan, *Mater. Adv.* **2020**, *1*, 648–657.
[38] J. Yan, X. Liu, B. Li, *Adv. Sci.* **2016**, *3*, 1600101.
[39] Y. Peng, R. Badam, T. P. Jayakumar, W. Wannapakdee, C. Changtong, N. Matsumi, *J. Electrochem. Soc.* **2022**, *169*, 050515.
[40] V. Knap, D.-I. Stroe, M. Swierczynski, R. Teodorescu, E. Schaltz, *J. Electrochem. Soc.* **2016**, *163*, A911–A916.
[41] Q. Fan, B. Li, Y. Si, Y. Fu, *Chem. Commun.* **2019**, *55*, 7655–7658.
[42] H. Lu, Z. Chen, H. Du, K. Zhang, J. Wang, Z. Hou, J. Fang, *Ionics (Kiel).* **2019**, *25*, 2685–2691.
[43] C. Monroe, J. Newman, *J. Electrochem. Soc.* **2003**, *150*, A1377.
[44] S. Suriyakumar, M. Kathiresan, A. M. Stephan, *ACS Omega.* **2019**, *4*, 3894–3903.
[45] N. A. Cañas, K. Hirose, B. Pascucci, N. Wagner, K. A. Friedrich, R. Hiesgen, *Electrochim. Acta.* **2013**, *97*, 42–51.
[46] Z. Ji, B. Han, Q. Li, C. Zhou, Q. Gao, K. Xia, J. Wu, *J. Phys. Chem. C.* **2015**, *119*, 20495–20502.
[47] Y. Zou, R. Chai, B. Yang, J. Li, D. Guo, H. Jin, Z. Yang, X. Chen, S. Wang, *Energy and Fuels.* **2021**, *35*, 13419–13425.
[48] X. Zhao, Z. Sun, Z. Yao, Z. Cui, J. Wang, T. Zhang, *J. Mater. Chem. A.* **2019**, *7*, 18237–18243.
[49] Y. Diao, K. Xie, S. Xiong, X. Hong, *J. Electrochem. Soc.* **2012**, *159*, A1816–A1821.
[50] V. S. Rangasamy, S. Thayumanasundaram, J.-P. Locquet, *Electrochim. Acta.* **2019**, *328*, 135133.
[51] M. J. Frisch, G. W. Trucks, H. B. Schlegel, G. E. Scuseria, M. A. Robb, J. R. Cheeseman, J. A. Montgomery Jr, T. Vreven, K. N. Kudin, J. C. Burant, J. M. Millam, S. S. Iyengar, J. Tomasi, V. Barone, B. Mennucci, M. Cossi, G. Scalmani, N. Rega, G. A. Petersson, H. Nakatsuji, M. Hada, M. Ehara, K. Toyota, R. Fukuda, J. Hasegawa, M. Ishida, T. Nakajima, Y. Honda, O. Kitao, H. Nakai, M. Klene, X. Li, J. E. Knox, H. P. Hratchian, J. B. Cross, C. Adamo, J. Jaramillo, R. Gomperts, R. E. Stratmann, O. Yazyev, A. J. Austin, R. Cammi, C. Pomelli, J. W. Ochterski, P. Y. Ayala, K. Morokuma, G. A.Voth, P. Salvador, J. J. Dannenberg, V. G. Zakrzewski, S. Dapprich, A. D. Daniels, M. C. Strain, O. Farkas, D. K. Malick, A. D. Rabuck, K. Raghavachari, J. B. Fores-man, J. V. Ortiz, Q. Cui, A. G. Baboul, S. Clifford, J. Cioslowski, B. B. Stefanov, G.Liu, A. Liashenko, P. Piskorz, I. Komaromi, R. L. Martin, D. J. Fox, T. Keith, M. A. Al-Laham, C. Y. Peng, A. Nanayakkara, M. Challacombe, P. M. W. Gill, B. Johnson, W. Chen, M. W. Wong, C. Gonzalez, J. A. Pople, *Gaussian 09*, Rev - D.01.
[52] U. Reeta Felscia, B. J. M. Rajkumar, P. Sankar, R. Philip, M. Briget Mary, *Spectrochim. Acta Part A Mol. Biomol. Spectrosc.* **2017**, *184*, 286–293.
[53] J. Zhang, J. Yang, Z. Liu, B. Zheng, *ACS Omega.* **2021**, *6*, 4995–5000.
[54] T.-Z. Hou, W.-T. Xu, X. Chen, H.-J. Peng, J.-Q. Huang, Q. Zhang, *Angew. Chemie Int. Ed.* **2017**, *56*, 8178–8182.
[55] X. Chen, Y. Bai, C. Zhao, X. Shen, Q. Zhang, *Angew. Chem. Int. Ed.* **2020**, *59*, 11192–11195.

Manuscript received: September 26, 2023
Revised manuscript received: November 13, 2023
Accepted manuscript online: November 24, 2023
Version of record online: December 12, 2023